Performance Evaluation of Navigation Using LEO Satellite Signals with Periodically Transmitted Satellite Positions

Christian T. Ardito, Joshua J. Morales, Joe J. Khalife, Ali A. Abdallah, and Zaher M. Kassas
University of California, Irvine

BIOGRAPHIES

Christian T. Ardito received a B.S. in Electrical Engineering from the University of Califorina, Riverside (UCR). He is currently pursuing a Ph.D. at the University of Califorina, Irvine (UCI) and is a member of the Autonomous Systems Perception, Intelligence, and Navigation (ASPIN) Laboratory. His research interests include satellite-based navigation, sensor fusion, and software-defined radio.

Joshua J. Morales is a Ph.D. student at UCI and a member of the ASPIN Laboratory. He received a B.S. in Electrical Engineering with High Honors from UCR. In 2016 he was accorded an Honorable Mention from the National Science Foundation (NSF). His research interests include estimation theory, navigation systems, autonomous vehicles, and intelligent transportation systems.

Joe J. Khalife is a Ph.D. student at UCI and member of the ASPIN Laboratory. He received a B.E. in Electrical Engineering and an M.S. in Computer Engineering from the Lebanese American University (LAU). From 2012 to 2015, he was a research assistant at LAU. His research interests include opportunistic navigation, autonomous vehicles, and software-defined radio.

Ali A. Abdallah is a Ph.D student at UCI and a member of the ASPIN Laboratory. He received a B.E in Electrical Engineering from LAU. His current research interests include opportunistic navigation and software-defined radio.

Zaher (Zak) M. Kassas is an assistant professor in the Department of Mechanical and Aerospace Engineering and the Department of Electrical Engineering and Computer Science at UCI and the Director of the ASPIN Laboratory. He received a B.E. in Electrical Engineering from LAU, an M.S. in Electrical and Computer Engineering from The Ohio State University, and an M.S.E. in Aerospace Engineering and a Ph.D. in Electrical and Computer Engineering from The University of Texas at Austin. In 2018, he received the National Science Foundation (NSF) Faculty Early Career Development Program (CAREER) award, and in 2019, he received the Office of Naval Research (ONR) Young Investigator Program (YIP) award. His research interests include cyber-physical systems, estimation theory, navigation systems, autonomous vehicles, and intelligent transportation systems.

ABSTRACT

The navigation performance with low Earth orbit (LEO) satellite signals is evaluated. The navigation framework used to perform this evaluation tightly integrates a vehicle's inertial navigation system (INS) with Doppler and pseudorange measurements from LEO satellites. The following scenario is considered. A vehicle has access to global navigation satellite system (GNSS) signals and *a priori*, uncertain information about LEO satellite states. The vehicle navigates by tightly integrating GNSS pseudorange measurements with its onboard INS. During the period when GNSS signals are available, the vehicle tracks the LEO satellites from pseudorange and Doppler measurements, refining estimates about their states. Next, GNSS signals are assumed to be unavailable. The vehicle transitions to a simultaneous tracking and navigation (STAN) mode where it simultaneously tracks the LEO satellites and navigates by integrating pseudorange and Doppler measurements made on the LEO satellites with its onboard INS. The performance of this navigation framework is evaluated for two cases: when the LEO satellites periodically transmit their position and when the do not transmit such information. Simulation results with existing LEO satellite constellations pertaining to Orbcomm and Globalstar as well as the future satellite constellation pertaining to Starlink are presented. It was assumed that the LEO satellites are periodically transmitting their positions. These simulation results consider an unmanned aerial vehicle (UAV) equipped with a tactical-grade inertial measurement unit (IMU) navigating for 81.6 km in 600 seconds, in which GNSS signals were only available for the first 100 seconds. It is demonstrated

Preprint of the 2019 ION ITM Conference Reston, VA, January 28–31, 2019

that the final position error of the INS-Orbcomm-Globalstar system was 93.01 m while the INS-Starlink system was 9.81 m. The position root mean squared error (RMSE) of the INS-Orbcomm-Globalstar system was 58.59 m while the INS-Starlink system was 10.13 m. Experimental results with existing Orbcomm LEO satellites are presented in which only Doppler measurements were made on two available satellites. The experimental results were conducted on a ground vehicle equipped with a tactical-grade IMU that traversed 7.5 km in 258 seconds, in which GNSS signals were only available for the first 30 seconds. It is demonstrated that the final position error of the INS without GNSS signals was 3.73 km and the position RMSE was 1.42 km. On the other hand, the final position error of the INS-Orbcomm system was 233.3 m and the position RMSE was 188.6 m when the position of the satellite was decoded from its transmitted message. If such position was not decoded and was estimated only from the STAN framework, the final position error was 476.3 m and the position RMSE was 195.6 m.

I. INTRODUCTION

Positioning systems that integrate signals from a global navigation satellite system (GNSS) and inertial navigation system (INS) take advantage of the complementary properties of each individual system: the INS has short-term accuracy and high data rates and the GNSS solution provides long-term, stable periodic corrections. However, in the inevitable event when GNSS signals become (i) unavailable (e.g., in deep urban canyons, near dense foliage, and in the presence of interference or jamming) or (ii) are ignored due to being untrustworthy (e.g., during malicious spoofing attacks), the INS's errors will grow unboundedly.

Signals of opportunity (SOPs) have been considered as an alternative navigation source in the absence of GNSS signals [1–4]. SOPs include AM/FM radio [5, 6], cellular [7, 8], digital television [9, 10], and low Earth orbit (LEO) satellites [11–14]. These signals have been demonstrated to yield a standalone meter-level-accurate navigation solution on ground vehicles [15–18] and a centimeter-level-accurate navigation solution on aerial vehicles [19, 20]. Moreover, these signals have been used as an aiding source for lidar [21, 22] and INS [23, 24].

LEO satellites are particularly attractive aiding sources for a vehicle's INS in GNSS-challenged environments for several reasons: (i) they are around twenty-times closer to Earth compared to GNSS satellites which reside in medium Earth orbit (MEO), making their received signals between 300 to 2,400 times more powerful than GNSS signals; (ii) thousands of broadband Internet satellites will be launched into LEO by OneWeb, Boeing, SpaceX (Starlink), among others, bringing an abundance of signal sources [25]; and (iii) each broadband provider will deploy satellites into unique orbital constellations transmitting at different frequency bands, making their signals diverse in frequency and direction [26].

To use transmissions from LEO satellites as SOPs for navigation, space vehicle (SV) positions and clock states must be determined. The positions of LEO SVs cannot be accurately predicted by their osculating orbital elements alone due to a multitude of time-varying forces, which cause trajectory deviations. Nonetheless, there are models that can propagate the orbital elements of satellites in space that take into account the various perturbations on the SVs. For instance, the simplified general perturbations 4 (SGP4) model uses two-line element (TLE) files that contain orbital elements and corrective terms to initialize and propagate the position of an SV [27]. This model generates predictions with errors as large as three-kilometers, 24-hours after a TLE is produced. Consequently, TLEs are produced daily by the North American Aerospace Defense Command (NORAD) to support the on-going usage of SGP4 as an orbit determination method. There also exist precise orbit determination (POD) methods that yield accurate ephemerides with errors on the order of tens-of-meters, in the radial, along-track, and cross-track directions for an SV, with more error occurring in the along-track direction [28, 29].

The exploitation of LEO satellites for navigation has been considered in other contexts. In [30], simulated LEO satellite Doppler measurements from known satellite positions were used to complement a cellular radio frequency pattern matching algorithm for localizing emergency 911 callers. In [31], simulated Doppler measurements from one LEO satellite with known position and velocity were used to localize a receiver. In [32], the position, velocity, and clock errors of a receiver were estimated using simulated LEO satellite time-difference of arrival (TDOA) and frequency difference of arrival (FDOA) measurements using a reference receiver with a known position.

This paper evaluates the performance of navigation with pseudorange and Doppler measurements from LEO SVs. The navigation framework considers aiding the INS onboard a vehicle with LEO SV pseudorange and Doppler measurements in a tightly-coupled fashion. A similar presentation of this framework was given in [33, 34]. In

contrast, to [33, 34], this paper studies the achieved performance whenever the LEO SVs periodically transmit their positions. The following scenario is considered. A vehicle has access to global navigation satellite system (GNSS) signals and *a priori*, uncertain information about LEO satellite states. The vehicle navigates by tightly integrating GNSS pseudorange measurements with its onboard INS. During the period when GNSS signals are available, the vehicle tracks the LEO satellites from pseudorange and Doppler measurements, refining estimates about their states. Next, GNSS signals are assumed to be unavailable. The vehicle transitions to a simultaneous tracking and navigation (STAN) mode where it simultaneously tracks the LEO satellites and navigates by integrating pseudorange and Doppler measurements made on the LEO satellites with its onboard INS. The performance of this navigation framework is evaluated for two cases: when the LEO satellites periodically transmit their position and when the do not transmit such information. Simulation results with existing LEO satellite constellations pertaining to Orbcomm and Globalstar as well as the future satellite constellation pertaining to Starlink are presented. It was assumed that the LEO satellites are periodically transmitting their positions. These simulation results consider an unmanned aerial vehicle (UAV) equipped with a tactical-grade inertial measurement unit (IMU) navigating for 81.6 km in 600 seconds, in which GNSS signals were only available for the first 100 seconds. It is demonstrated that the final position error of the INS-Orbcomm-Globalstar system was 93.01 m while the INS-Starlink system was 9.81 m. The position root mean squared error (RMSE) of the INS-Orbcomm-Globalstar system was 58.59 m while the INS-Starlink system was 10.13 m. Experimental results with existing Orbcomm LEO satellites are presented in which only Doppler measurements were made on two available satellites. The experimental results were conducted on a ground vehicle equipped with a tactical-grade IMU that traversed 7.5 km in 258 seconds, in which GNSS signals were only available for the first 30 seconds. It is demonstrated that the final position error of the INS without GNSS signals was 3.73 km and the position RMSE was 1.42 km. On the other hand, the final position error of the INS-Orbcomm system was 233.3 m and the position RMSE was 188.6 m when the position of the satellite was decoded from its transmitted message. If such position was not decoded and was estimated only from the STAN framework, the final position error was 476.3 m and the position RMSE was 195.6 m.

The remainder of this paper is organized as follows. Section II describes the LEO SOP-aided INS framework and discusses the LEO satellite dynamics model and the receiver measurement model. Section III provides an overview of the proposed Starlink constellation, which is used for simulation purposes. Section IV presents simulation results for an aerial vehicle navigating with the proposed framework with existing Orbcomm and Globalstar constellations as well as the proposed Starlink constellation. Section V presents experimental results for a ground vehicle navigating with the framework with existing Orbcomm SVs. Section VI presents concluding remarks.

II. FRAMEWORK DESCRIPTION

An extended Kalman filter (EKF) is employed to aid the INS with LEO SV pseudorange and Doppler in a tightly-coupled fashion. The EKF will also use GNSS pseudoranges, when available. The proposed STAN framework, illustrated in Fig. 1, works similarly to that of a traditional tightly-coupled GNSS-aided INS with two main differences: (i) the position and clock states of the LEO satellites are unknown to the vehicle-mounted receiver; hence, they are estimated simultaneously with the states of the navigating vehicle and (ii) pseudorange and/or Doppler measurements are used to aid the INS instead of GNSS pseudoranges. The positions of the SVs are propagated via an orbit determination method, which uses a simplified LEO SV dynamics model. The LEO SV states are initialized from TLE files. A similar framework was proposed in [23] to aid a vehicle's INS using stationary terrestrial emitters. The framework presented in this paper is more complex since it includes a LEO SV dynamics model to propagate the positions of moving LEO SVs. The EKF state vector, state dynamics model, receiver's measurement model, and the EKF prediction and measurement update are discussed next.

A. EKF State Vector

The EKF state vector is given by

$$\boldsymbol{x} = \left[\boldsymbol{x}_{\mathrm{r}}^{\mathsf{T}}, \boldsymbol{x}_{\mathrm{leo}_1}^{\mathsf{T}}, \ldots, \boldsymbol{x}_{\mathrm{leo}_M}^{\mathsf{T}} \right]^{\mathsf{T}} \tag{1}$$

$$\boldsymbol{x}_{\mathrm{r}} = \left[{}^{B}_{G}\bar{\boldsymbol{q}}^{\mathsf{T}}, \boldsymbol{r}_{\mathrm{r}}^{\mathsf{T}}, \dot{\boldsymbol{r}}_{\mathrm{r}}^{\mathsf{T}}, \boldsymbol{b}_{\mathrm{g}}^{\mathsf{T}}, \boldsymbol{b}_{\mathrm{a}}^{\mathsf{T}}, c\delta t_{\mathrm{r}}, c\dot{\delta} t_{\mathrm{r}} \right]^{\mathsf{T}} \tag{2}$$

$$\boldsymbol{x}_{\mathrm{leo}_m} = \left[\boldsymbol{r}_{\mathrm{leo}_m}^{\mathsf{T}}, \dot{\boldsymbol{r}}_{\mathrm{leo}_m}^{\mathsf{T}}, c\delta t_{\mathrm{leo}_m}, c\dot{\delta} t_{\mathrm{leo}_m} \right]^{\mathsf{T}} \tag{3}$$

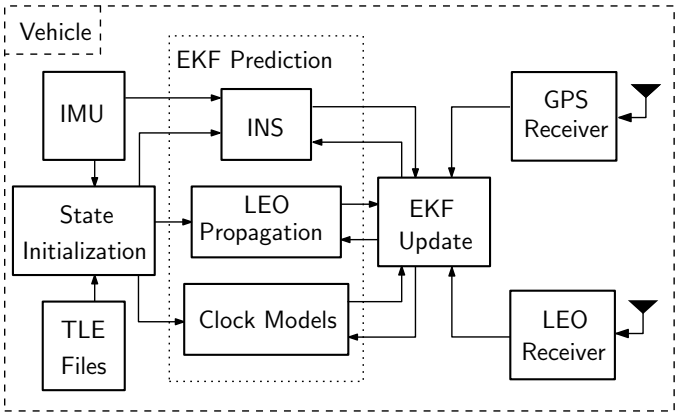

Fig. 1. Simultaneous LEO satellite tracking and navigation framework

where $\boldsymbol{x}_{\mathrm{r}}$ is the state vector of the vehicle-mounted IMU and receiver which consists of ${}^{B}_{G}\bar{\boldsymbol{q}}$, which is a four-dimensional (4-D) unit quaternion representing the orientation of a body frame B fixed at the IMU with respect to a global frame G; $\boldsymbol{r}_{\mathrm{r}}$ and $\dot{\boldsymbol{r}}_{\mathrm{r}}$ are the three-dimensional (3-D) position and velocity vector of the IMU; $\boldsymbol{b}_{\mathrm{g}}$ and $\boldsymbol{b}_{\mathrm{a}}$ are 3-D biases of the IMU's gyroscope and accelerometer, respectively; δt_{r} and $\dot{\delta} t_{\mathrm{r}}$ are the clock bias and drift of the receiver, respectively; and c is the speed of light. The vector $\boldsymbol{x}_{\mathrm{leo_m}}$ is the state vector of the m^{th} LEO SV, which consists of $\boldsymbol{r}_{\mathrm{leo_m}}$ and $\dot{\boldsymbol{r}}_{\mathrm{leo_m}}$, which are the 3-D satellite position and velocity, respectively; $\delta t_{\mathrm{leo_m}}$ and $\dot{\delta} t_{\mathrm{leo_m}}$ are the SV's transceiver clock bias and drift, respectively; and $m = 1, \ldots, M$, with M being the total number of LEO SVs that are visible to the receiver.

B. Vehicle Dynamics Model

The vehicle's orientation, position, and velocity are modeled to evolve in time according to INS kinematic equations driven by a 3-D rotation rate vector ${}^{B}\boldsymbol{\omega}$ of the body frame and a 3-D acceleration vector ${}^{G}\boldsymbol{a}$ in the global frame [35]. The gyroscope's and accelerometer's biases are modeled to evolve according to

$$\boldsymbol{b}_{\mathrm{g}}(k+1) = \boldsymbol{b}_{\mathrm{g}}(k) + \boldsymbol{w}_{\mathrm{bg}}(k), \tag{4}$$

$$\boldsymbol{b}_{\mathrm{a}}(k+1) = \boldsymbol{b}_{\mathrm{a}}(k) + \boldsymbol{w}_{\mathrm{ba}}(k), \quad k = 1, 2, \ldots, \tag{5}$$

where $\boldsymbol{w}_{\mathrm{bg}}$ and $\boldsymbol{w}_{\mathrm{ba}}$ are process noise vectors, which are modeled as a discrete-time white noise sequences with covariances $\mathbf{Q}_{\mathrm{bg}}$ and $\mathbf{Q}_{\mathrm{ba}}$, respectively. The vehicle-mounted receiver's clock error states are assumed to evolve in time according to

$$\boldsymbol{x}_{\mathrm{clk_r}}(k+1) = \mathbf{F}_{\mathrm{clk}}\, \boldsymbol{x}_{\mathrm{clk_r}}(k) + \boldsymbol{w}_{\mathrm{clk_r}}(k), \quad k = 1, 2, \ldots, \tag{6}$$

$$\boldsymbol{x}_{\mathrm{clk_r}} \triangleq \left[\, c\delta t_{\mathrm{r}},\, c\dot{\delta} t_{\mathrm{r}} \,\right]^{\mathsf{T}}, \quad \mathbf{F}_{\mathrm{clk}} = \begin{bmatrix} 1 & T \\ 0 & 1 \end{bmatrix},$$

where $\boldsymbol{w}_{\mathrm{clk_r}}$ is the process noise, which is modeled as a discrete-time white noise sequence with covariance

$$\mathbf{Q}_{\mathrm{clk_r}} = \begin{bmatrix} S_{\tilde{w}_{\delta t_{\mathrm{r}}}} T + S_{\tilde{w}_{\dot{\delta} t_{\mathrm{r}}}} \frac{T^3}{3} & S_{\tilde{w}_{\dot{\delta} t_{\mathrm{r}}}} \frac{T^2}{2} \\ S_{\tilde{w}_{\dot{\delta} t_{\mathrm{r}}}} \frac{T^2}{2} & S_{\tilde{w}_{\dot{\delta} t_{\mathrm{r}}}} T \end{bmatrix}, \tag{7}$$

and T is the constant sampling interval [36]. The terms $S_{\tilde{w}_{\delta t_{\mathrm{r}}}}$ and $S_{\tilde{w}_{\dot{\delta} t_{\mathrm{r}}}}$ are the clock bias and drift process noise power spectra, respectively, which can be related to the power-law coefficients, $\{h_{\alpha,\mathrm{r}}\}_{\alpha=-2}^{2}$, which have been shown through laboratory experiments to characterize the power spectral density of the fractional frequency deviation of an oscillator from nominal frequency according to $S_{\tilde{w}_{\delta t_{\mathrm{r}}}} \approx \frac{h_{0,\mathrm{r}}}{2}$ and $S_{\tilde{w}_{\dot{\delta} t_{\mathrm{r}}}} \approx 2\pi^2 h_{-2,\mathrm{r}}$ [37].

C. LEO Satellite Dynamics Model

The position and velocity dynamics of the m^{th} LEO SV are modeled as the sum of the two-body motion model equation and other perturbing accelerations, given by

$$\ddot{\boldsymbol{r}}_{\mathrm{leo_m}}(t) = -\frac{\mu}{\|\boldsymbol{r}_{\mathrm{leo_m}}(t)\|_2^3} \boldsymbol{r}_{\mathrm{leo_m}}(t) + \tilde{\boldsymbol{a}}_{\mathrm{leo_m}}(t), \tag{8}$$

where $\ddot{\boldsymbol{r}}_{\text{leo}_\text{m}} = \frac{d}{dt}\dot{\boldsymbol{r}}_{\text{leo}_\text{m}}$, i.e., the acceleration of the m^{th} LEO SV, $\mu = 398,600\ \text{km}^3/\text{s}^2$ is the standard gravitational parameter; and $\tilde{\boldsymbol{a}}_{\text{leo}_\text{m}}$ captures the overall perturbation in acceleration, which includes perturbations caused by non-uniform Earth gravitational field, atmospheric drag, solar radiation pressure, third-body gravitational forces (e.g., gravity of the Moon and Sun), and general relativity [28]. The perturbation vector $\tilde{\boldsymbol{a}}_{\text{leo}_\text{m}}$ is modeled as a white random process with power spectral density $\mathbf{Q}_{\tilde{a}_{\text{leo}_\text{m}}}$. The m^{th} LEO SV's clock error states time evolution are modeled according to

$$\boldsymbol{x}_{\text{clk}_{\text{leo,m}}}(k+1) = \mathbf{F}_{\text{clk}}\, \boldsymbol{x}_{\text{clk}_{\text{leo,m}}}(k) + \boldsymbol{w}_{\text{clk}_{\text{leo,m}}}(k), \quad k = 1, 2, \ldots, \tag{9}$$

where $\boldsymbol{w}_{\text{clk}_{\text{leo,m}}}$ is a discrete-time white noise sequence with covariance of identical structure to $\mathbf{Q}_{\text{clk}_\text{r}}$ in (7), except that $S_{\tilde{w}_{\delta t_\text{r}}}$ and $S_{\tilde{w}_{\dot{\delta} t_\text{r}}}$ are replaced with the LEO SV clock specific spectra $S_{\tilde{w}_{\delta t_{\text{leo},m}}}$ and $S_{\tilde{w}_{\dot{\delta} t_{\text{leo},m}}}$, respectively, where $S_{\tilde{w}_{\delta t_{\text{leo},m}}} \approx \frac{h_{0,\text{leo}_\text{m}}}{2}$ and $S_{\tilde{w}_{\dot{\delta} t_{\text{leo},m}}} \approx 2\pi^2 h_{-2,\text{leo}_\text{m}}$. The next subsection discusses how these models are used in the EKF prediction.

D. IMU Measurement Model and EKF Prediction

The vehicle-mounted IMU, which contains a triad-gyroscope and triad-accelerometer, produces angular rate $\boldsymbol{\omega}_{\text{imu}}$ and specific force $\boldsymbol{a}_{\text{imu}}$ measurements, which are modeled as

$$\boldsymbol{\omega}_{\text{imu}}(k) = {}^{B}\boldsymbol{\omega}(k) + \boldsymbol{b}_\text{g}(k) + \boldsymbol{n}_\text{g}(k), \tag{10}$$

$$\boldsymbol{a}_{\text{imu}}(k) = \mathbf{R}\left[{}^{B_k}_{G}\bar{\boldsymbol{q}}(k)\right]\left({}^{G}\boldsymbol{a}(k) - {}^{G}\boldsymbol{g}(k)\right) + \boldsymbol{b}_\text{a}(k) + \boldsymbol{n}_\text{a}(k), \quad k = 1, 2, \ldots, \tag{11}$$

where ${}^{G}\boldsymbol{g}$ is the acceleration due to gravity in the global frame and $\boldsymbol{n}_\text{g}$ and $\boldsymbol{n}_\text{a}$ are measurement noise vectors, which are modeled as white noise sequences with covariances $\sigma_\text{g}^2\mathbf{I}_{3\times3}$ and $\sigma_\text{a}^2\mathbf{I}_{3\times3}$, respectively.

The EKF prediction produces $\hat{\boldsymbol{x}}(k|j) \triangleq \mathbb{E}[\boldsymbol{x}(k)|\boldsymbol{Z}^j]$ of $\boldsymbol{x}(k)$, and an associated estimation error covariance $\mathbf{P}_{\boldsymbol{x}}(k|j)$, where $\mathbb{E}[\cdot|\cdot]$ is the conditional expectation operator, $\boldsymbol{Z}^j \triangleq \{\hat{\boldsymbol{z}}(i)\}_{i=1}^{j}$ are the set of measurements available up to and including time index j, and $k > j$. The measurements $\boldsymbol{z}$ will be discussed in the next subsection.

The IMU measurements (10) and (11) are processed through strapdown INS equations using an Earth-centered Earth-fixed (ECEF) frame as frame G to produce ${}^{B}_{G}\hat{\bar{\boldsymbol{q}}}(k|j)$, $\hat{\boldsymbol{r}}_\text{r}(k|j)$, and $\hat{\dot{\boldsymbol{r}}}_\text{r}(k|j)$ [38]. The gyroscope's and accelerometer's biases predictions $\hat{\boldsymbol{b}}_\text{g}(k|j)$ and $\hat{\boldsymbol{b}}_\text{a}(k|j)$ can be readily calculated utilizing (4) and (5), respectively. The prediction of the clock states of both the receiver and the LEO SV transceivers can be readily calculated utilizing (6) and (9), respectively. The prediction of the LEO SV's position and velocity is performed by linearizing and discretizing (8). Next, the measurement model and the EKF measurement update is described.

E. Receiver Measurement Model and EKF Update

The GNSS receiver makes pseudorange measurements on all available GNSS satellites, which after compensating for ionospheric and tropospheric delays are modeled as

$$z_{\text{gnss}_\text{l}}(j) = \|\boldsymbol{r}_\text{r}(j) - \boldsymbol{r}_{\text{gnss}_\text{l}}(j)\|_2 + c\cdot\left[\delta t_\text{r}(j) - \delta t_{\text{gnss}_\text{l}}(j)\right] + v_{\text{gnss}_\text{l}}(j), \quad j = 1, 2, \ldots, \tag{12}$$

where $z_{\text{gnss}_\text{l}} \triangleq z'_{\text{gnss}_\text{l}} - c\delta t_{\text{iono}} - c\delta t_{\text{tropo}}$; δt_{iono} and δt_{tropo} are the ionospheric and tropospheric delays, respectively; $z'_{\text{gnss}_\text{l}}$ is the uncompensated pseudorange; v_{gnss_l} is the measurement noise, which is modeled as a discrete-time zero-mean white Gaussian sequence with variance $\sigma^2_{\text{z}_{\text{gnss,l}}}$; $l = 1, \ldots, L$; and L is the total number of GNSS SVs.

The LEO receiver makes Doppler frequency measurements f_D on LEO SV signals, from which a pseudorange rate measurement $\dot{\rho}$ can be obtained from $\dot{\rho} = -\frac{c}{f_c}f_D$, where f_c is the carrier frequency. The pseudorange rate measurement $\dot{\rho}_{\text{leo}_m}$ from the m^{th} LEO satellite is modeled according to

$$\begin{aligned}\dot{\rho}_{\text{leo}_m}(j) = {} & [\dot{\boldsymbol{r}}_{\text{leo}_m}(j) - \dot{\boldsymbol{r}}_r(j)]^{\mathsf{T}}\, \frac{[\boldsymbol{r}_r(j) - \boldsymbol{r}_{\text{leo}_m}(j)]}{\|\boldsymbol{r}_r(j) - \boldsymbol{r}_{\text{leo}_m}(j)\|_2} \\ & + c\cdot\left[\dot{\delta}t_r(j) - \dot{\delta}t_{\text{leo}_m}(j)\right] + c\dot{\delta}t_{\text{iono}_m}(j) \\ & + c\dot{\delta}t_{\text{trop}_m}(j) + v_{\dot{\rho}_m}(j), \quad j = 1, 2, \ldots, \quad m = 1, \ldots, M,\end{aligned}$$

where $\dot{\delta}t_{\text{iono}_m}$ and $\dot{\delta}t_{\text{trop}_m}$ are the drifts of the ionospheric and tropospheric delays, respectively, for the m^{th} LEO SV and $v_{\dot{\rho}_m}$ is the measurement noise, which is modeled as a white Gaussian random sequence with variance $\sigma^2_{\dot{\rho}_{\text{leo,m}}}$. Note that the variation in the ionospheric and tropospheric delays during LEO SV visibility is negligible compared to the errors in the satellite's estimated velocities [39]; hence, $\dot{\delta}t_{\text{iono}_m}$ and $\dot{\delta}t_{\text{trop}_m}$ are ignored in the measurement, yielding the measurement model given by

$$\begin{aligned}\dot{\rho}_{\text{leo}_m}(j) =& [\dot{\boldsymbol{r}}_{\text{leo}_m}(j) - \dot{\boldsymbol{r}}_r(j)]^{\mathsf{T}} \frac{[\boldsymbol{r}_r(j) - \boldsymbol{r}_{\text{leo}_m}(j)]}{\|\boldsymbol{r}_r(j) - \boldsymbol{r}_{\text{leo}_m}(j)\|_2} \\ &+ c \cdot \left[\dot{\delta}t_r(j) - \dot{\delta}t_{\text{leo}_m}(j)\right] + v_{\dot{\rho}_m}(j). \quad j = 1, 2, \ldots, \quad m = 1, \ldots, M, \end{aligned} \tag{13}$$

The LEO receiver also makes pseudorange measurements on LEO SVs, which are modeled as

$$z_{\text{leo}_\text{m}}(j) = \|\boldsymbol{r}_\text{r}(j) - \boldsymbol{r}_{\text{leo}_\text{m}}(j)\|_2 + c \cdot [\delta t_\text{r}(j) - \delta t_{\text{leo}_\text{m}}(j)] + v_{\text{leo}_\text{m}}(j), \quad j = 1, 2, \ldots, \tag{14}$$

The navigation framework operates in (i) a tracking mode when GNSS measurements are available and (ii) a STAN mode when GNSS signals are unavailable. In the tracking mode, the measurement vector $\boldsymbol{z}$ processed by the EKF update is defined by stacking all available GNSS pseudoranges and LEO satellite pseudorange and Doppler measurements and is given by

$$\boldsymbol{z} \triangleq \left[\boldsymbol{z}_{\text{gnss}}^{\mathsf{T}}, \dot{\boldsymbol{\rho}}_{\text{leo}}^{\mathsf{T}}, \boldsymbol{z}_{\text{leo}}^{\mathsf{T}}\right]^{\mathsf{T}}, \tag{15}$$

$$\boldsymbol{z}_{\text{gnss}} \triangleq \left[z_{\text{gnss}_1}, \ldots, z_{\text{gnss}_\text{L}}\right]^{\mathsf{T}}, \quad \dot{\boldsymbol{\rho}}_{\text{leo}} \triangleq \left[\dot{\rho}_{\text{leo}_1}, \ldots, \dot{\rho}_{\text{leo}_\text{M}}\right]^{\mathsf{T}}, \quad \boldsymbol{z}_{\text{leo}} \triangleq \left[z_{\text{leo}_\text{m}}, \ldots, z_{\text{leo}_\text{M}}\right]^{\mathsf{T}}.$$

In the STAN mode, GNSS signals are unavailable and the measurement vector $\boldsymbol{z}$ becomes

$$\boldsymbol{z} \triangleq \left[\dot{\boldsymbol{\rho}}_{\text{leo}}^{\mathsf{T}}, \boldsymbol{z}_{\text{leo}}^{\mathsf{T}}\right]^{\mathsf{T}}. \tag{16}$$

F. Periodically Transmitted LEO SV Position Model

It is assumed that the LEO SVs are equipped with GNSS receivers, enabling them to estimate their position, which then gets periodically transmitted down to Earth. The vehicle-mounted LEO receiver decodes this transmitted position, which is modeled as

$$\boldsymbol{z}_{\text{orb,m}}(k) = \boldsymbol{r}_{\text{leo,m}}(k) + \boldsymbol{v}_{\text{orb,m}}(k), \quad k = 1, 2, \ldots, \tag{17}$$

where $\boldsymbol{v}_{\text{orb,m}}$ models the uncertainty in the LEO SV's position, which is assumed to be a zero-mean white gaussian sequence with covariance $\mathbf{Q}_{\text{orb,m}} = \text{diag}\left[\sigma^2_{\text{ra}}, \sigma^2_{\text{at}}, \sigma^2_{\text{ct}}\right]$. The next section provides an overview of SpaceX's proposed Starlink satellite constellation from which Doppler and pseudorange measurements were simulated to aid an INS in Section IV.

III. STARLINK OVERVIEW

In this section, an overview of the proposed Starlink constellation is given according to filings SpaceX has made to the Federal Communications Commission (FCC) [40–42]. The currently approved Starlink satellite constellation is discussed and details are given about requested modifications.

A. Proposed Starlink Constellation

The Starlink satellite communication system is an ambitious project by SpaceX to provide the Earth with global Internet access. The Starlink system can be broken into segments consisting of SVs in LEO and very low Earth orbit (VLEO), ground control and gateway facilities, and user terminals. The current number of approved SVs is 11,943, which when launched, would more than double the amount of objects ever launched into outer space according to the United Nations Office for Outer Space Affairs (8,303 objects were listed on November 29, 2018 [43]).

SpaceX indicated in their original filing that service for licensed users will begin after the first 800 satellites are deployed. Furthermore, the FCC places milestone requirements on licensees developing satellite constellations, such as SpaceX, to launch and operate half of the proposed constellation within six-years of grant approval. Therefore, Starlink should become operational for users by 2024. Table I describes the most recently approved orbital configuration for the LEO and VLEO sub-constellations. It should be noted that SpaceX has requested to remove the 1,600 SVs at 1,150 km and replace them with 1,584 SVs at 550 km [42]. If approved, these SVs at 550 km would be the first deployment of SVs supported by Starlink. Fig. 2 shows the LEO sub-constellation over Earth.

TABLE I
STARLINK ORBITAL CONFIGURATION

	LEO Constellation					VLEO Constellation		
Satellites per Altitude	1600	1600	400	375	450	2547	2478	2493
Altitude (km)	1150	1110	1130	1275	1325	354.6	340.8	335.9
Inclination (°)	53	53.8	74	81	70	53	48	42

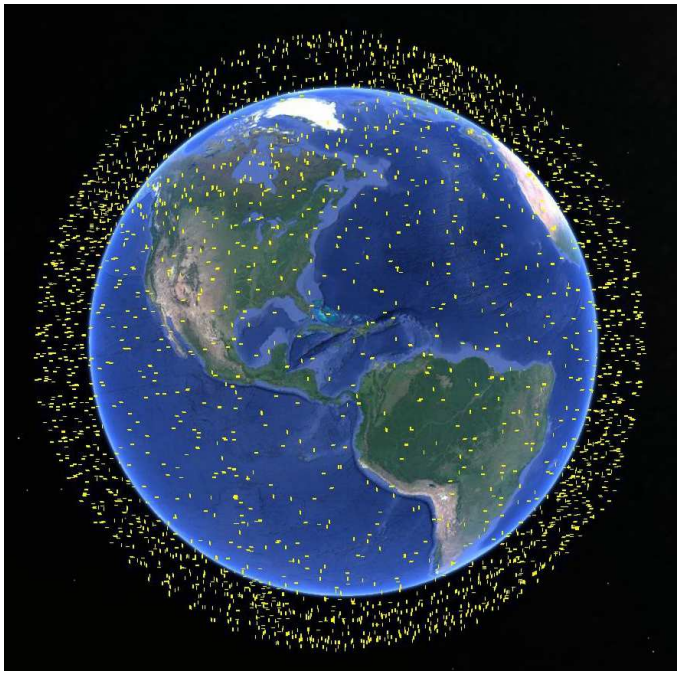

Fig. 2. Visualization of proposed LEO Starlink satellites. Map data: Google Earth

B. Signal Information

Users will be able to communicate with Starlink SVs once the SVs exceed a 35° elevation angle. Starlink has permission to transmit in the Ku, Ka, and V-bands. User terminals will have phased array antennas with up to 8×16 elements using half- wavelength spacing, thus antenna apertures designed for V-band communication are expected to be approximately 20 cm^2. Steered antenna beams will track SVs to aid communication links between user terminals and LEO SVs. Additionally, downlink V-band beacon signals using between 1 and 10 MHz of spectrum will facilitate rapid SV acquisition as handovers occur. Downlink signal beams will support both left and right hand polarizations and channel bandwidths of 50 MHz on the Ku-band and 1 GHz on the V-band.

The next section demonstrates the achievable navigation performance using simulated IMU data and simulated pseudorange and Doppler measurements on Starlink SVs.

IV. SIMULATION RESULTS

In this section, the LEO signal-aided INS framework is analyzed by simulating Starlink Doppler and pseudorange measurements made from a UAV-mounted receiver. Performance using the proposed LEO Starlink constellation is compared against performance attainable from the existing LEO Orbcomm and Globalstar constellations.

A. General Simulation Settings

In all the following simulations, a UAV equipped with a tactical-grade IMU and GPS and LEO SV receivers navigates for 81.6 km in ten-minutes . The UAV has access to GPS pseudoranges for the first 100 seconds. For the remaining 500 seconds, the UAV navigates using its LEO SOP-aided INS only. After lift-off, the UAV makes ten banking turns. Pseudorange and Doppler measurements are taken at 10 Hz; GPS pseudoranges, while available, are taken at 1 Hz; and the IMU measurements are made at 100 Hz. It is assumed that the LEO SVs periodically transmit their positions at 1 Hz according to (17). The initial states of the UAV and the LEO SVs are initialized as $\hat{\boldsymbol{x}}_{\mathrm{r}}(0|0) \sim \mathcal{N}[\boldsymbol{x}_{\mathrm{r}}(0), \mathbf{P}_{\mathrm{r}}(0|0)]$ and $\hat{\boldsymbol{x}}_{\mathrm{leo}_m}(0|0) \sim \mathcal{N}[\boldsymbol{x}_{\mathrm{leo}_m}(0), \mathbf{P}_{\mathrm{leo_m}}(0|0)]$. The estimation error covariances are initialized as

$$\mathbf{P}_{\mathrm{r}}(0|0) \equiv \mathrm{blkdiag}\left[\mathbf{P}_{\substack{B\\G}\bar{\boldsymbol{q}}}(0|0),\, \mathbf{P}_{\boldsymbol{r}_{\mathrm{r}}}(0|0),\, \mathbf{P}_{\dot{\boldsymbol{r}}_{\mathrm{r}}}(0|0),\, \mathbf{P}_{\boldsymbol{b}_{\mathrm{g}}}(0|0),\, \mathbf{P}_{\boldsymbol{b}_{\mathrm{a}}}(0|0),\, \mathbf{P}_{\boldsymbol{x}_{\mathrm{r_{clk}}}}(0|0)\right]$$
$$\mathbf{P}_{\mathrm{leo_m}}(0|0) \equiv \mathrm{blkdiag}\left[\mathbf{P}_{\boldsymbol{r}_{\mathrm{leo_m}}}(0|0),\, \mathbf{P}_{\dot{\boldsymbol{r}}_{\mathrm{leo_m}}}(0|0),\, \mathbf{P}_{\boldsymbol{x}_{\mathrm{leo_{m_{clk}}}}}(0|0)\right],$$

where blkdiag denotes a block diagonal matrix. The UAV-mounted receiver is assumed to be equipped with a temperature-compensated crystal oscillator (TCXO), while the LEO SVs are assumed to be equipped with oven-controlled crystal oscillators (OCXOs). Table II summarizes the simulation settings. Note, the initial LEO error covariance matrices below, $\mathbf{P}_{\boldsymbol{r}_{\mathrm{leo,body_m}}}(0|0)$ and $\mathbf{P}_{\dot{\boldsymbol{r}}_{\mathrm{leo,body_m}}}(0|0)$, are provided for convenience in the satellite body frame corresponding to the radial, along-track, and cross-track directions; $\boldsymbol{r}_{\mathrm{leo}}$ is defined in the ECEF frame.

TABLE II
SIMULATION ERROR SETTINGS

Parameter	Value
$\mathbf{P}_{\substack{B\\G}\bar{\boldsymbol{q}}}(0\|0)$	$10^{-3} \cdot \mathrm{diag}\,[1,\, 1,\, 1]$
$\mathbf{P}_{\boldsymbol{r}_{\mathrm{r}}}(0\|0)$	$9 \cdot \mathrm{diag}\,[1,\, 1,\, 1]$
$\mathbf{P}_{\dot{\boldsymbol{r}}_{\mathrm{r}}}(0\|0)$	$\mathrm{diag}\,[1,\, 1,\, 1]$
$\mathbf{P}_{\boldsymbol{b}_{\mathrm{g}}}(0\|0)$	$10^{-6} \cdot \mathrm{diag}\,[1,\, 1,\, 1]$
$\mathbf{P}_{\boldsymbol{b}_{\mathrm{a}}}(0\|0)$	$10^{-6} \cdot \mathrm{diag}\,[1,\, 1,\, 1]$
$\mathbf{P}_{\boldsymbol{x}_{\mathrm{r_{clk}}}}(0\|0)$	$\mathrm{diag}\,[6,\, 1]$
$\mathbf{P}_{\boldsymbol{r}_{\mathrm{leo,body_m}}}(0\|0)$	$\mathrm{diag}\left[10^2,\, 100^2,\, 10^2\right]$
$\mathbf{P}_{\dot{\boldsymbol{r}}_{\mathrm{leo,body_m}}}(0\|0)$	$10^{-2} \cdot \mathrm{diag}\,[1,\, 1,\, 1]$
$\mathbf{P}_{\boldsymbol{x}_{\mathrm{leo_{clk_m}}}}(0\|0)$	$\mathrm{diag}\,[1,\, 0.1]$
$\mathbf{Q}_{\mathrm{orb,body_m}}$	$\mathrm{diag}\left[1.45^2,\, 0.67^2,\, 0.56^2\right]$
$\{h_{0,\mathrm{r}},\, h_{-2,\mathrm{r}}\}$	$\left\{9.4 \times 10^{-20},\, 3.8 \times 10^{-21}\right\}$
$\{h_{0,\mathrm{leo_m}},\, h_{-2,\mathrm{leo_m}}\}_{m=1}^{M}$	$\left\{8.0 \times 10^{-20},\, 4.0 \times 10^{-23}\right\}$

B. LEO Constellation Comparisons

This subsection investigates the achievable navigation performance with the existing Orbcomm and Globalstar constellations versus that of the proposed Starlink constellation. Here, the performance metrics are 3-D final position error and root mean-squared error (RMSE). During the course of the Starlink simulation, there were a total of 78 LEO SVs that passed within the 35° elevation mask set by the UAV, with an average of 27 SVs available at any point in time. This simulation does not include the recently approved VLEO Starlink SVs. In comparison, 12 SVs in

total from the Orbcomm and Globalstar constellations passed within an 18° elevation mask set by the UAV, with an average of 6 SVs available at any point in time. A total of 143 Orbcomm and Globalstar SVs were simulated; however, it should be noted that the number of actively transmitting SVs from these constellations is 71 SVs, according to the active SV list from [27].

Fig. 3 shows the 3σ uncertainties and estimation error trajectories for the UAV's position and velocity for the three different runs: (i) without INS aiding, (ii) with INS aiding from Orbcomm and Globalstar pseudorange and Doppler measurements, and (iii) with INS aiding from Starlink pseudorange and Doppler measurements. As expected, after GNSS cutoff, the errors of the unaided INS grow rapidly unboundedly. In contrast, aiding with Orbcomm and Globalstar SV signals reduces the error growth and seems to bound it, albeit at high values. On the other hand, aiding with Starlink SV signals, bounds and reduces the error at much lower values. This is due to the higher number of Starlink SVs compared to Orbcomm and Globalstar. Table III summarizes the UAV's navigation performance over the ten-minute trajectory shown in Fig. 4.

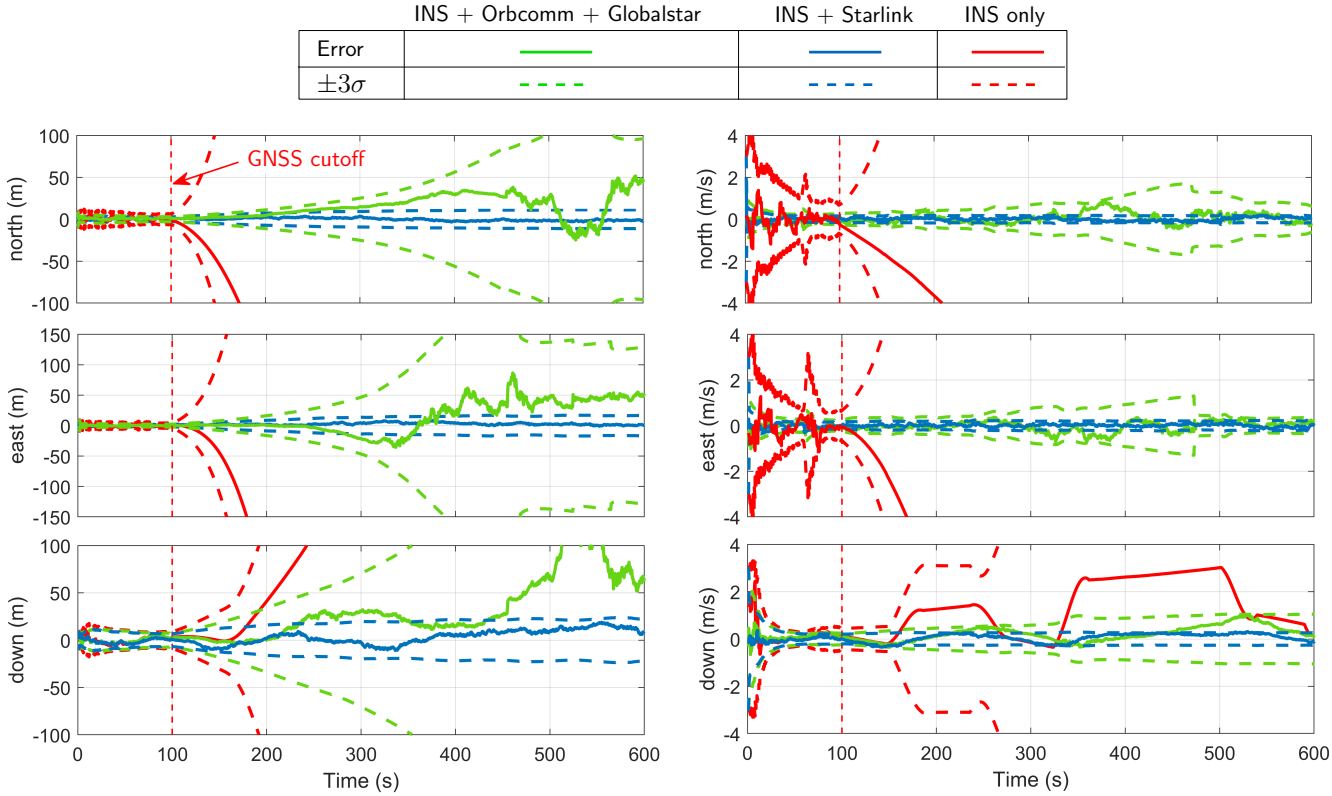

Fig. 3. Simulation results showing the UAV's position and velocity estimation error trajectories and 3σ uncertainties for the ten-minute flight duration, during which GNSS signals were only available for the first 100 seconds.

TABLE III
UAV Navigation Performance

Performance Measure	INS only	INS + Orbcomm + Globalstar	INS + Starlink
RMSE (m)	6,864.6	58.59	10.13
Final Error (m)	16,589	93.01	9.81

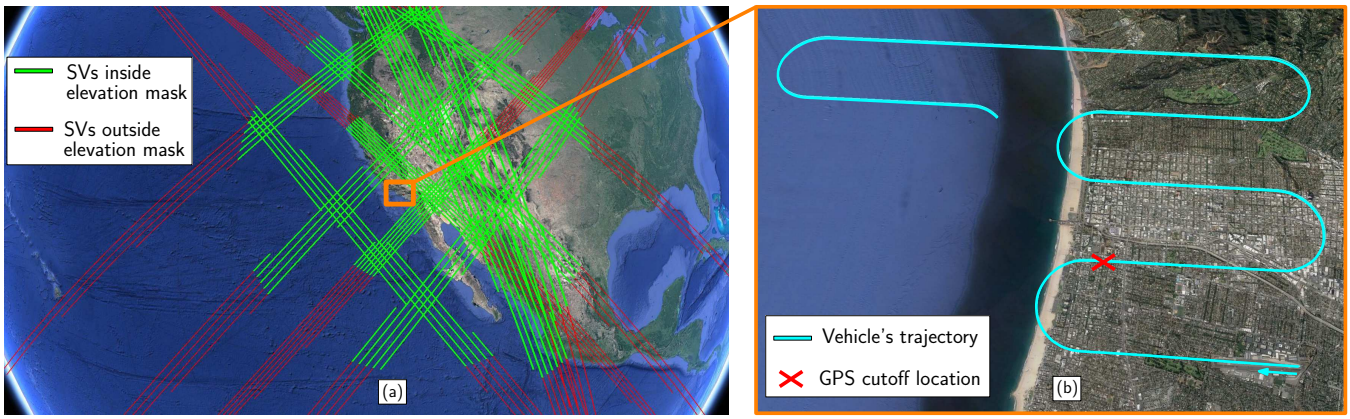

Fig. 4. Simulation environment: (a) LEO Starlink SV trajectories. (b) UAV's trajectories. Map data: Google Earth

V. EXPERIMENTAL RESULTS

In this section, the LEO signal-aided INS framework is presented through an experiment using signals from Orbcomm LEO SVs. Doppler measurements and SV positions were collected from Orbcomm downlink signals, which contain SV ephemeris messages. These ephemerides are determined by GNSS receivers onboard the SVs. A receiver was designed to measure Doppler and decode the SVs' positions from the transmitted message. This section compares the achievable performance with and without using the SVs' postions in the framework discussed in Section II.

A. Experimental Setup

A ground vehicle was equipped with the following hardware and software setup:

- A quadrifilar helix antenna to receive the Orbcomm SV downlink signals, which are transmitted at frequencies between 137 and 138 MHz.
- A USRP E312 to sample Orbcomm symmetric differential phase shift keying (SDPSK) signals.
- These samples were then processed by the Multi-channel Adaptive TRansceiver Information eXtractor (MATRIX) software-defined radio developed by the Autonomous Systems Perception, Intelligence, and Navigation (ASPIN) Laboratory to perform carrier synchronization, extract pseudorange rate observables, and decode Orbcomm ephemeris messages [44].
- A Septentrio AsteRx-i V integrated GNSS-IMU, which is equipped with a dual-antenna, multi-frequency GNSS receiver and a Vectornav VN-100 micro-electromechanical system (MEMS) IMU. Septentrio's post-processing software development kit (PP-SDK) was used to process GPS carrier phase observables collected by the AsteRx-i V and by a nearby differential GPS base station to obtain a carrier phase-based navigation solution. This integrated GNSS-IMU real-time kinematic (RTK) system [45] was used to produce the ground truth results with which the proposed navigation framework was compared.

The experimental setup is shown in Fig. 5.

B. Results

The ground vehicle was driven along U.S. Interstate 5 near Irvine, California for 7,495 km over 258 seconds, during which 2 Orbcomm LEO satellites were available. The standard deviation of the Orbcomm Doppler measurements was set to be 4.7 Hz, which was obtained empirically. Three navigation frameworks were implemented to estimate the vehicle's trajectory: (i) the LEO signal-aided INS STAN framework described in Section II, (ii) the LEO signal-aided INS STAN framework without the periodically transmitted SV positions, (iii) a traditional GPS-aided INS for comparative analysis.

Each framework had access to GPS for only the first 30 seconds of the run as illustrated in Fig. 6 (d). Fig. 6 (a) shows the trajectory the 2 Orbcomm LEO satellites traversed over the course of the experiment. Table IV summarizes

the navigation performance. The estimated satellite trajectory and the along-track, radial, and cross-track 99$^{\text{th}}$-percentile final uncertainty ellipsoid for one of the Orbcomm SVs are illustrated in Fig. 6 (b) for the case where SV position updates were transmitted periodically. It is worth noting that the performance in the experimental results is worse than that in the simulation results due to the significantly lower number of LEO SVs from which only Doppler measurements were used.

TABLE IV
GROUND VEHICLE NAVIGATION PERFORMANCE

Performance Measure	**INS only**	**INS + Orbcomm without position updates**	**INS + Orbcomm with position updates**
RMSE (m)	1,419	195.6	188.6
Final Error (m)	3,729	476.3	233.3

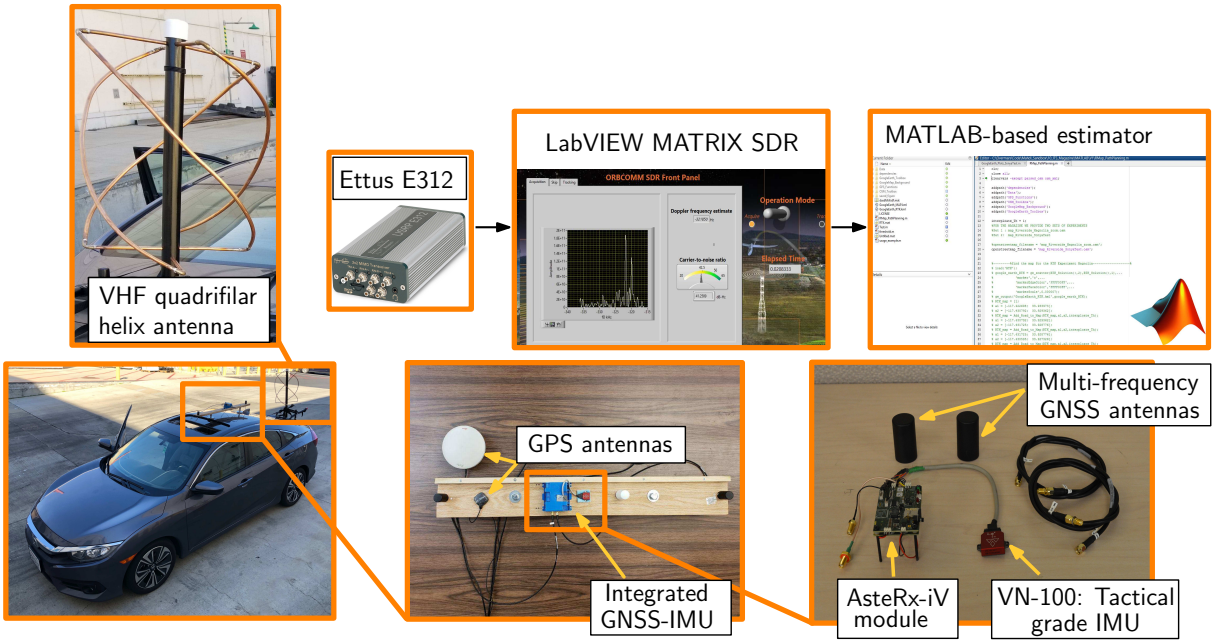

Fig. 5. Experimental setup.

VI. CONCLUSIONS

This work presented a framework to navigate with LEO SV signals. The framework aids the INS onboard an aerial or a ground vehicle with pseudorange and Doppler measurements in the absence of GNSS signals. The framework considered the case where the LEO SVs transmit their own positions. Simulation results comparing the achievable performance of the existing Orbcomm and Globalstar LEO constellations versus that of the proposed Starlink constellation was presented. The simulations considered a UAV equipped with a tactical-grade IMU traveling for 81.6 km in ten-minutes, during which GNSS signals were only available for the first 100 seconds. The RMSE of the INS-Orbcomm-Globalstar system was 58.59 m while it was 10.13 m for the INS-Starlink system. Moreover, experimental results demonstrated the achievable performance on a ground vehicle traveling for 7.5 km in 258 seconds, during which GPS signals were only available for the first 30 seconds. Only Doppler measurements from 2 Orbcomm SVs were used and a comparison was conducted to evaluate the achievable performance with and without using SVs' transmitted positions in the framework. The RMSE of the unaided INS was 1,419 m and the final position error was 3,729 m. Without LEO SV position updates, the position RMSE was 195.6 m and the final position error was 476.3 m. With LEO SV position updates, the position RMSE was 188.6 m and the final position error was 233.3 m.

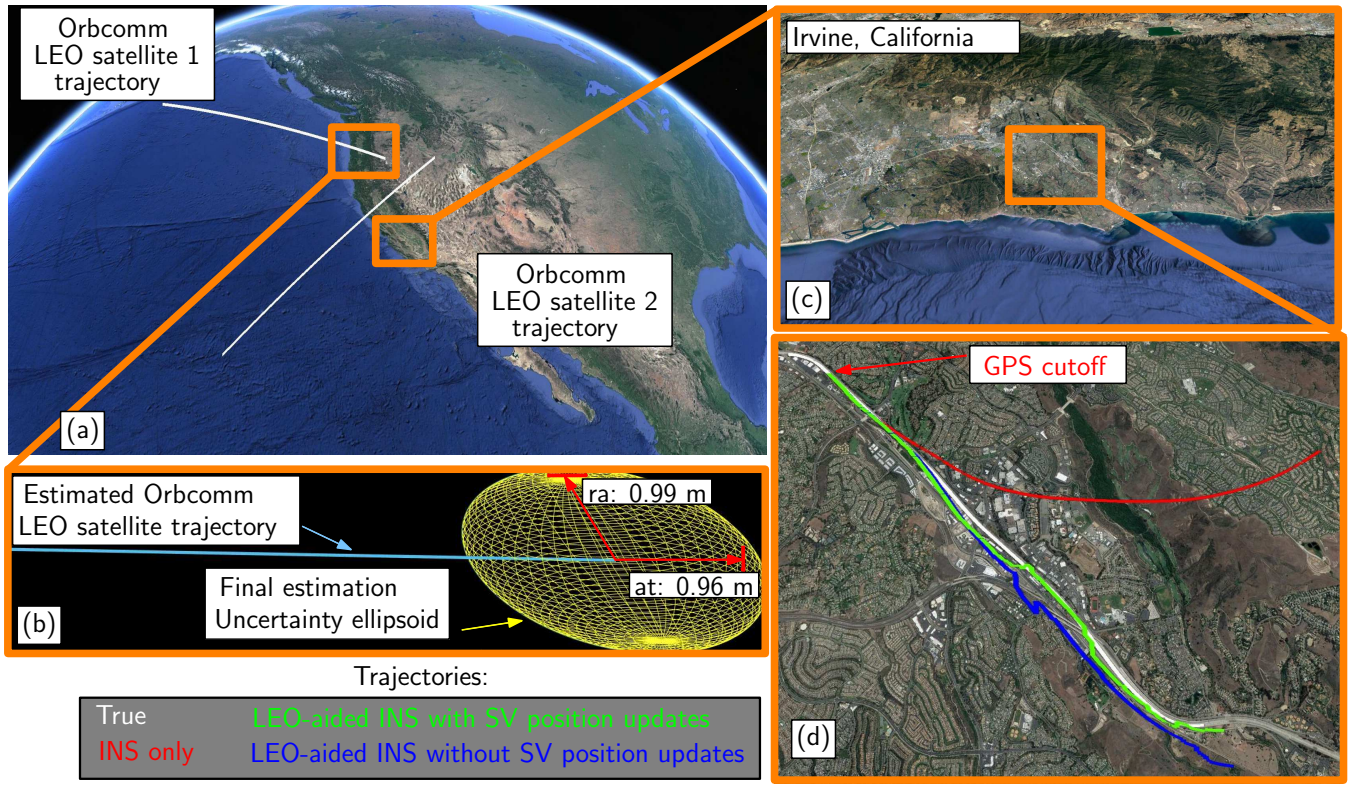

Fig. 6. Experimental results showing (a) the trajectory of the 2 Orbcomm LEO satellites, (b) estimated trajectory of one of the satellites and the final position uncertainty, and (c)–(d) true and estimated trajectories of the ground vehicle. Map data: Google Earth

Acknowledgment

This work was supported in part by the Office of Naval Research (ONR) under Grant N00014-16-1-2305 and in part by the National Science Foundation (NSF) under Grant 1751205.

References

[1] J. Raquet and R. Martin, "Non-GNSS radio frequency navigation," in *Proceedings of IEEE International Conference on Acoustics, Speech and Signal Processing*, March 2008, pp. 5308–5311.

[2] L. Merry, R. Faragher, and S. Schedin, "Comparison of opportunistic signals for localisation," in *Proceedings of IFAC Symposium on Intelligent Autonomous Vehicles*, September 2010, pp. 109–114.

[3] Z. Kassas, "Collaborative opportunistic navigation," *IEEE Aerospace and Electronic Systems Magazine*, vol. 28, no. 6, pp. 38–41, 2013.

[4] Z. Kassas, "Analysis and synthesis of collaborative opportunistic navigation systems," Ph.D. dissertation, The University of Texas at Austin, USA, 2014.

[5] J. McEllroy, "Navigation using signals of opportunity in the AM transmission band," Master's thesis, Air Force Institute of Technology, Wright-Patterson Air Force Base, Ohio, USA, 2006.

[6] S. Fang, J. Chen, H. Huang, and T. Lin, "Is FM a RF-based positioning solution in a metropolitan-scale environment? A probabilistic approach with radio measurements analysis," *IEEE Transactions on Broadcasting*, vol. 55, no. 3, pp. 577–588, September 2009.

[7] Z. Kassas, J. Khalife, K. Shamaei, and J. Morales, "I hear, therefore I know where I am: Compensating for GNSS limitations with cellular signals," *IEEE Signal Processing Magazine*, pp. 111–124, September 2017.

[8] K. Shamaei, J. Khalife, and Z. Kassas, "Exploiting LTE signals for navigation: Theory to implementation," *IEEE Transactions on Wireless Communications*, vol. 17, no. 4, pp. 2173–2189, April 2018.

[9] M. Rabinowitz and J. Spilker, Jr., "A new positioning system using television synchronization signals," *IEEE Transactions on Broadcasting*, vol. 51, no. 1, pp. 51–61, March 2005.

[10] P. Thevenon, S. Damien, O. Julien, C. Macabiau, M. Bousquet, L. Ries, and S. Corazza, "Positioning using mobile TV based on the DVB-SH standard," *NAVIGATION, Journal of the Institute of Navigation*, vol. 58, no. 2, pp. 71–90, 2011.

[11] M. Rabinowitz, B. Parkinson, C. Cohen, M. O'Connor, and D. Lawrence, "A system using LEO telecommunication satellites for rapid acquisition of integer cycle ambiguities," in *Proceedings of IEEE/ION Position Location and Navigation Symposium*, April 1998, pp. 137–145.

[12] M. Joerger, L. Gratton, B. Pervan, and C. Cohen, "Analysis of Iridium-augmented GPS for floating carrier phase positioning," *NAVIGATION, Journal of the Institute of Navigation*, vol. 57, no. 2, pp. 137–160, 2010.

[13] K. Pesyna, Z. Kassas, and T. Humphreys, "Constructing a continuous phase time history from TDMA signals for opportunistic navigation," in *Proceedings of IEEE/ION Position Location and Navigation Symposium*, April 2012, pp. 1209–1220.

[14] T. Reid, A. Neish, T. Walter, and P. Enge, "Leveraging commercial broadband LEO constellations for navigating," in *Proceedings of ION GNSS Conference*, September 2016, pp. 2300–2314.
[15] C. Yang, T. Nguyen, and E. Blasch, "Mobile positioning via fusion of mixed signals of opportunity," *IEEE Aerospace and Electronic Systems Magazine*, vol. 29, no. 4, pp. 34–46, April 2014.
[16] J. Khalife and Z. Kassas, "Navigation with cellular CDMA signals – part II: Performance analysis and experimental results," *IEEE Transactions on Signal Processing*, vol. 66, no. 8, pp. 2204–2218, April 2018.
[17] M. Driusso, C. Marshall, M. Sabathy, F. Knutti, H. Mathis, and F. Babich, "Vehicular position tracking using LTE signals," *IEEE Transactions on Vehicular Technology*, vol. 66, no. 4, pp. 3376–3391, April 2017.
[18] K. Shamaei and Z. Kassas, "LTE receiver design and multipath analysis for navigation in urban environments," *NAVIGATION, Journal of the Institute of Navigation*, vol. 65, no. 4, pp. 655–675, December 2018.
[19] J. Khalife and Z. Kassas, "Precise UAV navigation with cellular carrier phase measurements," in *Proceedings of IEEE/ION Position, Location, and Navigation Symposium*, April 2018, pp. 978–989.
[20] J. Khalife, K. Shamaei, S. Bhattacharya, and Z. Kassas, "Centimeter-accurate UAV navigation with cellular signals," in *Proceedings of ION GNSS Conference*, September 2018, accepted.
[21] J. Khalife, S. Ragothaman, and Z. Kassas, "Pose estimation with lidar odometry and cellular pseudoranges," in *Proceedings of IEEE Intelligent Vehicles Symposium*, June 2017, pp. 1722–1727.
[22] M. Maaref, J. Khalife, and Z. Kassas, "Lane-level localization and mapping in GNSS-challenged environments by fusing lidar data and cellular pseudoranges," *IEEE Transactions on Intelligent Vehicles*, 2018, accepted.
[23] J. Morales, P. Roysdon, and Z. Kassas, "Signals of opportunity aided inertial navigation," in *Proceedings of ION GNSS Conference*, September 2016, pp. 1492–1501.
[24] Z. Kassas, J. Morales, K. Shamaei, and J. Khalife, "LTE steers UAV," *GPS World Magazine*, vol. 28, no. 4, pp. 18–25, April 2017.
[25] T. Reid, A. Neish, T. Walter, and P. Enge, "Broadband LEO constellations for navigation," *NAVIGATION, Journal of the Institute of Navigation*, vol. 65, no. 2, pp. 205–220, 2018.
[26] D. Lawrence, H. Cobb, G. Gutt, M. OConnor, T. Reid, T. Walter, and D. Whelan, "Navigation from LEO: Current capability and future promise," *GPS World Magazine*, vol. 28, no. 7, pp. 42–48, July 2017.
[27] North American Aerospace Defense Command (NORAD), "Two-line element sets," http://celestrak.com/NORAD/elements/.
[28] J. Vetter, "Fifty years of orbit determination: Development of modern astrodynamics methods," *Johns Hopkins APL Technical Digest*, vol. 27, no. 3, pp. 239–252, November 2007.
[29] D. Vallado, "An analysis of state vector propagation using differing flight dynamics programs," in *Proceedings of the AAS Space Flight Mechanics Conference*, vol. 120, January 2005.
[30] D. Qiu, D. Lorenzo, and T. Bhattacharya, "Indoor geo-location with cellular rf pattern matching and LEO communication satellite signals," in *Proceedings of ION International Technical Meeting Conference*, January 2013, pp. 726–733.
[31] X. Chen, M. Wang, and L. Zhang, "Analysis on the performance bound of Doppler positioning using one LEO satellite," in *Proceedings of IEEE Vehicular Technology Conference*, May 2016, pp. 1–5.
[32] J. Zhao, L. Li, and Y. Gong, "Joint navigation and synchronization in LEO dual-satellite geolocation systems," in *Proceedings of IEEE Vehicular Technology Conference*, June 2017, pp. 1–5.
[33] J. Morales, J. Khalife, A. Abdallah, C. Ardito, and Z. Kassas, "Inertial navigation system aiding with Orbcomm LEO satellite Doppler measurements," in *Proceedings of ION GNSS Conference*, September 2018, accepted.
[34] J. Morales, J. Khalife, C. Ardito, and Z. Kassas, "Simultaneous tracking of Orbcomm LEO satellites and inertial navigation system aiding using Doppler measurements," in *Proceedings of IEEE Vehicular Technology Conference*, 2019, accepted.
[35] J. Farrell and M. Barth, *The Global Positioning System and Inertial Navigation*. New York: McGraw-Hill, 1998.
[36] Z. Kassas and T. Humphreys, "Observability analysis of collaborative opportunistic navigation with pseudorange measurements," *IEEE Transactions on Intelligent Transportation Systems*, vol. 15, no. 1, pp. 260–273, February 2014.
[37] A. Thompson, J. Moran, and G. Swenson, *Interferometry and Synthesis in Radio Astronomy*, 2nd ed. John Wiley & Sons, 2001.
[38] P. Groves, *Principles of* GNSS*, Inertial, and Multisensor Integrated Navigation Systems*, 2nd ed. Artech House, 2013.
[39] P. Misra and P. Enge, *Global Positioning System: Signals, Measurements, and Performance*, 2nd ed. Ganga-Jamuna Press, 2010.
[40] SpaceX, "FCC File Number: SATLOA2016111500118," *IB FCC Report*, March 2018, accessed: November 29, 2018.
[41] SpaceX, "FCC File Number: SATLOA2017030100027," *IB FCC Report*, November 2018, accessed: November 29, 2018.
[42] SpaceX, "FCC File Number: SATMOD2018110800083," *IB FCC Report*, November 2018, accessed: November 29, 2018.
[43] UNOOSA, "Online index of objects launched into outer space," http://www.unoosa.org/oosa/osoindex/, November 2018, accessed: November 29, 2018.
[44] J. Khalife and Z. Kassas, "Receiver design for Doppler positioning with LEO satellites," in *Proceedings of IEEE International Conference on Acoustics, Speech and Signal Processing*, 2019, accepted.
[45] (2018) Septentrio AsteRx-i V. [Online]. Available: https://www.septentrio.com/products